# Surface-Roughness Induced Residual Stresses in Thermal Barrier Coatings: Computer Simulations

C. H. Hsueh[1], P. F. Becher[1],
Edwin R. Fuller, Jr.[2], Stephen A. Langer[2], and W. Craig Carter[3]

[1] Oak Ridge National Laboratory, Oak Ridge, Tennessee 37831-6068, U.S.A.
[2] National Institute of Standards and Technology, Gaithersburg, Maryland 20899, U.S.A.
[3] presently at Massachusetts Institute of Technology, Cambridge, MA 02139-4307, U.S.A.

**Keywords:** asperities; computer simulations; finite element analysis; microstructure; OOF; plasma spray; residual stress; spallation; surface roughness; thermal barrier coatings

## Abstract

Adherence of plasma-sprayed thermal barrier coatings (TBC's) is strongly dependent on mechanical interlocking at the interface between the ceramic coating and the underlying metallic bond coat. Typically, a rough bond-coat surface topology is required to achieve adequate mechanical bonding. However, the resultant interfacial asperities modify the residual stresses that develop in the coating system due to thermal expansion differences, and other misfit strains, and generate stresses that can induce progressive fracture and eventual spallation of the ceramic coating. For a flat interface, the principal residual stress is parallel to the interface, as the stress normal to the interface is zero. However, the residual stress normal to the interface becomes non-zero, when the interface has the required interlocking morphology. In the present study, an actual microstructure of a plasma-sprayed TBC system was numerically simulated and analyzed with a recently developed, object-oriented finite element analysis program, *OOF*, to give an estimate of the localized residual stresses in a TBC system. Additionally, model TBC microstructures were examined to evaluate the manner in which the topology of interfacial asperities influences residual stresses. Results are present for several scenarios of modifying interfacial roughness.

## Introduction

Ceramic thermal barrier coatings (TBC's) are commonly used to protect air-cooled superalloy hardware in hot-sections of gas turbine engines by reducing the surface temperatures of metallic components [1-4]. A typical plasma-sprayed TBC system consists of an oxidation-resistant metallic bond coat overlaid by a porous, thermally-insulating ceramic coating [1-3]. Since adherence of the plasma-sprayed ceramic coating to the metallic surface is enhanced by mechanical interlocking, a rough bond-coat surface topology is required to achieve the level of mechanical adhesion needed for the severe thermal cycles of a turbine engine [3,5,6]. Plasma-spray deposition of the bond coat provides an inherently rough and irregular metallic surface, with the resultant asperities providing good bonding along the ceramic/metal interface. Furthermore, the nature of the bond-coat surface-roughness can be tailored to a limited extent by control of plasma-spray parameters and/or powder size distributions. Currently, the magnitude and morphology of bond-coat roughness that provide optimum TBC durability have not been established.

Substantial residual stresses exist in TBC systems due to the large mismatch in metal-ceramic thermal expansion during cooling and to high-temperature oxidation of the bond coat [2-7]. During high-temperature operation, a thin oxide scale (predominantly, $\alpha$-$Al_2O_3$) forms at the irregular bond-coat/coating interface, resulting in a constrained volumetric increase along the interface [2-7]. The interfacial oxide scale and ceramic coating have significantly lower coefficients of thermal expansion (CTE) than the underlying metallic components, and thus, are subjected to significant compressive residual stresses parallel to the interface during cooling [4,8,9]. The residual stress normal to the interface (i.e., the out-

## DISCLAIMER

of-plane residual stress) would be zero if the interface were perfectly flat [10,11], but becomes non-zero, when asperities are present [11]. Fracture and/or buckling of the interfacial oxide scale and ceramic coating can occur during cooling as a result of the combined in-plane compression and out-of-plane tension, [2-4,8,9].

Plasma-spraying produces a lamellar microstructure, consisting of numerous, interlocked ceramic platelets that formed upon impact of the molten ceramic particles. Thus, the as-deposited ceramic coating contains a fine inter-lamellar porosity of numerous crack-like pores parallel to the interface [3,8]. Residual tensile stresses normal to the interface during repeated thermal cycling can result in the growth and coalescence of this crack-like porosity. Damage accumulation eventually results in failure by fracture and delamination of the ceramic coating near to and above the irregular, oxidized interface.

The purpose of the present study is to elucidate the influence of interface asperities on residual stress distributions in a plasma-sprayed TBC system at room temperature, particularly, the residual stresses normal to the interface. To achieve this, a recently developed, object-oriented finite element analysis program (*OOF*) was adopted [13]. *OOF* is designed to operate on microstructural images, thereby incorporating the actual microstructure of a material system. First, the microstructural constituents of a TBC system are described. Then, using an actual cross-sectional micrograph of this microstructure, residual stresses for the specific interface morphology and inter-lamellar porosity distribution of the microstructure were analyzed by *OOF*. To systematically examine the influence of interface asperities on the residual stress distributions, *OOF* was also used to study model microstructures with various interface geometries. Specifically, these model microstructures consisted of an oxidized TBC system with a periodic sinusoidal interface topology to simulate the bond-coat asperities. Additionally, the valley and peak portions of the sinusoidal topology were removed to examine separately the influence of convex and concave asperities. Effects of oxide scale thickness and the coating inter-lamellar porosity on residual stress distributions were also studied.

## The TBC System

The TBC system examined in this study consisted of an air plasma sprayed (APS) 8 wt% $Y_2O_3$ partially stabilized $ZrO_2$ (YSZ) coating deposited on a vacuum plasma sprayed (VPS) Ni-22Cr-10Al-1Y (NiCrAlY) bond coat [3]. The VPS NiCrAlY bond coat was fabricated in a manner that induced significant surface roughness (on the order of 14.2 μm $R_A$) to enhance adhesion of the YSZ coating [3]. The substrate is René N5, a single-crystal Ni-based superalloy. Thicknesses of the coating, bond coat, and substrate are ~200 μm, ~125 μm, and ~3.175 mm, respectively. A typical cross-section of this specimen is shown in Fig. 1a after 270 thermal cycles to 1150°C followed by forced-air cooling to ~90°C. A previous study determined that this number of

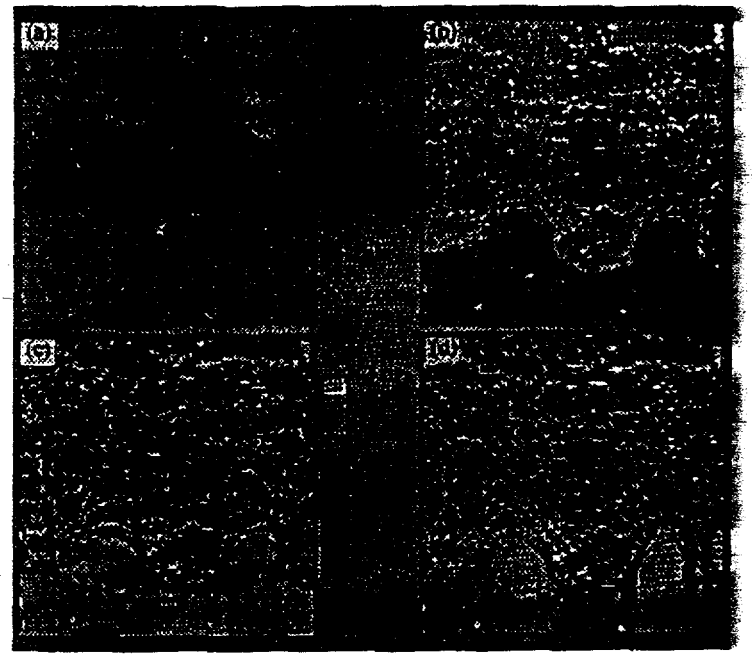


Figure 1. (a) Micrograph of TBC microstructure, (b) processed image for numerical simulations. Respectively, (c) and (d) are the calculated residual stresses, $\sigma_x$ and $\sigma_y$, for the plasma sprayed-$ZrO_2$ coating, the $\alpha$-$Al_2O_3$ oxidation scale, and the NiCrAlY bond coat. [The René N5 substrate is not shown.]

cycles represents approximately 75% of the average lifetime under these test conditions [12]. The dark contrast region in Fig. 1a between the porous ceramic coating and the dense metallic bond coat is the $\alpha$-$Al_2O_3$ scale (~5 μm in thickness). Large asperities are observed at the bond-coat interface due to its roughness. Inter-lamellar porosity and cracks are observed both within the coating and the oxide scale. The majority of the cracks are parallel to and near the bond-coat interface, as also observed in previous studies [5,6,7,9]. Although the crack distribution in the YSZ coating did not exhibit a clear trend, cracks in the interfacial oxide scale were predominately located on the *convex* portions of the interface asperities. The oxide scale was also typically thicker in these convex bond-coat regions. In many locations the interface scale consisted of multiple thinner layers of oxide sub-scale beneath the buckled original scale. Some localized regions of multi-layered scale were as thick as 20 μm [12]. The localized scale buckling and delamination are likely the result of a combination of large compressive residual stresses parallel to the interface and smaller tensile residual stresses normal to the interface.

## Numerical Simulations

Residual stresses were simulated using *OOF* [13], an object-oriented finite element program that operates on microstructural images. The present simulations used pixel-map representations of micrographs (i.e., a uniform rectangular array of colors, or greyscales, to describe the image) as inputs to *OOF*. Each pixel (or array element) becomes two triangular finite elements. Although the present analysis was two-dimensional, Young's modulus, $E$, was replaced by $E/(1-\nu)$, where $\nu$ is Poisson's ratio, to capture (approximately) the biaxial-stress nature of the dominate residual stress state for the TBC system (i.e., the stress parallel to the interface). Simulations were performed on an actual TBC microstructure to analyze its residual stresses and on several model microstructures to systematically elucidate influences of interfacial asperities and oxide scale thickness on residual stress distributions.

To analyze residual stresses in an actual TBC systems, the mismatch strains considered in the present study were the thermal and oxidation strains; stresses due to the plasma-spray deposition process were not considered. The thermal/mechanical properties used in the analyses are listed in Table 1 [2, 14]. Values for the coefficients of thermal expansion (CTE) were an average over the temperature range of 25°C to 1150°C. The temperature change used in calculating the thermal strain was -1125°C (i.e., 25°C - 1150°C). Any plastic and/or creep deformation of the bond coat was not considered. An exact determination of Young's modulus for the porous, micro-cracked ceramic coating (~200 μm thickness) is difficult. However, Young's moduli of 5 to 50 GPa have been reported for free-standing deposits of APS YSZ [2, 14]. In the present numerical simulation studies, the upper bound value 50 GPa was used for Young's modulus of the coating prior to incorporating cracks. Although oxidation strains are not explicitly included in *OOF*, they can be readily incorporated by replacing the CTE of the oxide scale with an effective CTE, such that the *effective* thermal strain is the sum of the actual thermal strain and the oxidation strain. However, since the magnitude of oxidation strains for TBC bond coats is not well documented, they were not included in the present study.

Table 1. Thermal/mechanical properties for the air-plasma sprayed YSZ ceramic coating, the $\alpha$-$Al_2O_3$ oxidation scale, the VPS NiCrAlY bond coat, and the René N5 substrate system.

| | Coating | Oxide Scale | Bond Coat | Substrate |
|---|---|---|---|---|
| Young's Modulus, $E$ (GPa) | 50 | 360 | 200 | 213 |
| Poisson's Ratio, $\nu$ | 0.10 | 0.27 | 0.30 | 0.25 |
| CTE (x $10^{-6}$/°C) | 10 | 8 | 15.2 | 14.5 |

***Analysis of an Actual Microstructure.*** The microstructure of Fig. 1a was digitized to a portable pixel map (.ppm) format. The processed image (consisting of 78,408 elements) is shown in Fig. 1b. The visible cracks were included in the analysis (see the empty elements in Fig. 1b). Since the substrate (not shown in Fig. 1) was much thicker than the other constituents, the thermal strain of the substrate (i.e., -1.63%)

was used as the boundary condition at the right and the left edges of the image in Fig. 1b to constrain its distortion in the $x$-direction.

Using *OOF*, the predicted stress-maps for $\sigma_x$ and $\sigma_y$ are shown in Figs. 1c and 1d, respectively. The stresses in the system, minus the cracks (represented by empty elements), are indicated by the greyscale bar in Fig. 1, which ranges from -1.5 GPa to +1.5 GPa. Statistical summaries of the residual stresses in each constituent (averaged over all elements) are listed in Table. 2. It is noted that in the absence of both interface asperities and cracks, $\sigma_x$ in the coating, the oxide scale, and the bond coat should be -281 MPa, -3,600 MPa, and 225 MPa respectively, and $\sigma_y$ should be zero. As expected, perturbation of the residual stress field due to the presence of interface asperities and cracks is obvious in Figs. 1c and 1d, with the averaged values presented in Table 2. Specifically, $\sigma_y$ is tensile in the convex portions with maximum tensile stresses of ~50 MPa, ~120 MPa, ~530 MPa in the coating, the oxide scale, and the bond coat, respectively. A question is thus raised as to whether the bond coat surface-roughness can be better designed to mitigate the tensile stress field normal to the interface, i.e., $\sigma_y$. To study this, numerical simulations were performed on model microstructures as follows.

Table 2. Statistics of the residual stresses, $\sigma_x$ and $\sigma_y$, of the microstructure in Fig. 1b.

| | Coating | Oxide Scale | Bond Coat |
|---|---|---|---|
| $\sigma_x$ (MPa) | -228±107 | -1543±1090 | 171±273 |
| $\sigma_y$ (MPa) | -2.5±49 | -739±855 | 179±354 |

***Analyses of Model Microstructures.*** Six model TBC microstructures were analyzed. First, an oxide scale with a periodic sinusoidal topology, simulating interface asperities, was evaluated (Fig. 2a). It is noted that this sinusoidal geometry has been adopted elsewhere [16-18] to evaluate TBC residual stress states. Second, the valley portion of the sinusoidal interface was removed to examine the role of convex asperities (Fig. 2b). Third, the peak portion of the sinusoidal interface was removed to examine the role of concave asperities (Fig. 2c). Fourth, the oxide scale was removed (Fig. 2d) to simulate the as-received TBC system prior to high-temperature exposure. Fifth, the oxide-scale thickness was doubled (Fig. 2e). Sixth, periodic arrays of cracks were inserted into the coating (Fig. 2f). The processed images for the model microstructures in Figs. 2a-2f each contained 41,472 finite elements.

Using *OOF*, predicted stress maps for $\sigma_x$ and $\sigma_y$ are also shown in Figs. 2a-2f for the six model microstructures. Statistics of $\sigma_x$ and $\sigma_y$ in the coating, the oxide scale, and the bond coat are listed in Table 3. The significant variations of the values in Table 3 are due to localized stress fluctuations along the irregular interfaces. It can be seen in Fig. 2a that tensile and compressive stresses normal to the interface, $\sigma_y$, occur in regions of convex and concave asperities, respectively. Without concave asperities (Fig. 2b), the large compressive stress concentration of $\sigma_y$ in the concave-asperity region in Fig. 2a spreads out to the flat-interface region (Fig. 2b). Without the convex asperities (Fig. 2c), the tensile stress of $\sigma_y$ in the convex-asperity region in Fig. 2a shifts to the flat-interface region (Fig. 2c). This occurs because there is no force applied in the $y$-direction. Consequently, the compressive values of $\sigma_y$ due to concave asperities require tensile values of $\sigma_y$ elsewhere (i.e., in the flat-interface region in this case) to achieve mechanical equilibrium. Statistics of the modeling results (see Table 3) suggest that it is beneficial to remove either the concave or the convex asperities in terms of reducing (1) the maximum tensile $\sigma_y$ in the coating as well as the bond coat, and (2) the stress fluctuation in the constituents. Effects of removing the concave and the convex asperities were similar. The models also indicate that it is detrimental to remove either the concave or convex asperities in terms of reducing compressive $\sigma_x$ in the oxide scale. However, reducing the stress levels in the thin interfacial scale is not likely a primary concern with regard to increasing the durability of plasma-sprayed TBC's. This is because prior studies have indicated that the fracture response of the interfacial scale does not play a dominant role in failure of high quality plasma-sprayed TBC's with adequate interface roughness [6,15].

In the absence of an oxide scale (Fig. 2d), the tensile $\sigma_y$ and its fluctuation in the bond coat are reduced; however, the maximum tensile stress, $\sigma_y$, in the coating increases. When the thickness of the oxide scale increases (Fig. 2e), the compressive $\sigma_y$ and its fluctuation decrease in both the coating and the oxide scale; however, the tensile $\sigma_y$ and its fluctuation increase in the bond coat. Finally, with cracks aligned parallel to the $x$-axis in the coating (Fig. 2f), $\sigma_y$ is relaxed, while $\sigma_x$ remains similar to that in the coating.

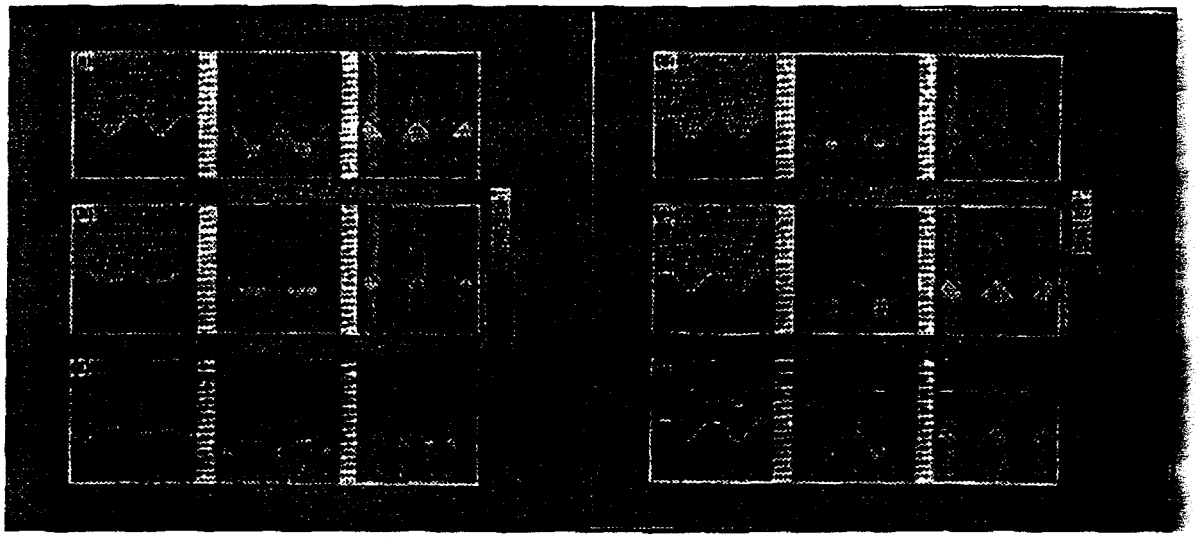

Fig. 2. Six model TBC microstructures and the calculated residual stresses, $\sigma_x$ and $\sigma_y$. (a) a sinusoidal interface topology with an oxide scale; (b) the valley portion of the sinusoidal topology is removed; (c) the peak portion of the sinusoidal topology is removed; (d) the oxide scale is removed; (e) the thickness of the oxide scale is doubled; and (f) periodic arrays of horizontal cracks are introduced into the coating.

Table 3. Statistics of residual stresses for model microstructures depicted in Figs. 2a-2f.

| Stresses in Coating | Sinusoidal Interface (Fig. 2a) | Valleys Removed (Fig. 2b) | Peaks Removed (Fig. 2c) | Scale Removed (Fig. 2d) | Scale Doubled (Fig. 2e) | Cracks Added (Fig. 2f) |
|---|---|---|---|---|---|---|
| $\sigma_x$ (MPa) | -284±26 | -283±24 | -284±26 | -276±21 | -287±36 | -283±31 |
| $\sigma_y$ (MPa) | -4±23 | -0.7±12.1 | -0.1±10.8 | -14±52 | -0.5±17.4 | -1.5±16.9 |

| Stresses in Oxide Scale | Sinusoidal Interface (Fig. 2a) | Valleys Removed (Fig. 2b) | Peaks Removed (Fig. 2c) | Scale Removed (Fig. 2d) | Scale Doubled (Fig. 2e) | Cracks Added (Fig. 2f) |
|---|---|---|---|---|---|---|
| $\sigma_x$ (MPa) | -2107±563 | -2555±661 | -2580±615 | NA | -2006±529 | -2116±564 |
| $\sigma_y$ (MPa) | -1091±804 | -659±734 | -589±711 | NA | -947±725 | -1104±817 |

| Stresses in Bond Coat | Sinusoidal Interface (Fig. 2a) | Valleys Removed (Fig. 2b) | Peaks Removed (Fig. 2c) | Scale Removed (Fig. 2d) | Scale Doubled (Fig. 2e) | Cracks Added (Fig. 2f) |
|---|---|---|---|---|---|---|
| $\sigma_x$ (MPa) | 201±142 | 217±114 | 222±125 | 189±94 | 192±169 | 199±143 |
| $\sigma_y$ (MPa) | 85±238 | 41±193 | 48±203 | 21±54 | 113±296 | 82±231 |

## Summary and Conclusions

Reliability of plasma-sprayed YSZ coatings is of major importance for the use of TBC's in high-temperature applications. However, the stress states which can lead to fracture and spallation of these ceramic coatings have not been fully analyzed and are not yet well understood. While a rough bond-coat surface is required to achieve good mechanical adhesion between coating and bond coat, the resulting interfacial asperities give rise to stresses which can lead to coating delamination. Thermal cycling experiments [12] on the TBC system analyzed in this study have shown that coating damage is cumulative in nature, with cracking and delamination of the ceramic layer occurring parallel to and near the irregular interface. Also, greater amounts of interfacial scale damage were observed in the vicinity of convex asperities, likely as a result of tensile residual stresses normal to the interface. While the residual stress normal to the interface, $\sigma_y$, is zero when the interface is flat, it is non-zero when the interface contains asperities. Specifically, $\sigma_y$ values in the ceramic layers are tensile in the convex-asperity region during cooling, since the bond coat has a greater coefficient of thermal expansion than the coating. The present study attempts to address the damage problem by analyzing the effects of interface asperities on residual stress distributions in the TBC system. It should be noted that this analysis did not consider the strain due to interfacial oxidation or time- and temperature-dependent mechanical response of the various TBC constituents.

The numerical simulation, *OOF*, run on the actual microstructure of the TBC system (Fig. 1a) shows that $\sigma_y$ is tensile in the region of convex asperities (Fig. 1d). To systematically examine effects of interface asperities on residual stress distributions, *OOF* was also run on model microstructures (Figs. 2a-2f). The simulated results from model microstructures provide preliminary guidelines for designing bond-coat surface roughness to minimize damage due to residual stresses. Since plasma-sprayed TBC systems tend to fail by spallation of the coating near the interface between the coating and the oxide scale, the surface-roughness design for the coating should focus on reducing both compressive $\sigma_x$ and tensile $\sigma_y$ in the coating close to the coating/oxide-scale interface while maintaining adequate mechanical adhesion. Based on the simulated results (Table 3), a logical choice to reduce the stresses would be to eliminate or reduce the convex asperities. However, this may concomitantly reduce the level of mechanical bonding between the coating and the bond coat, and would certainly present significant processing challenges.

Finally, effects of constituent thermal/mechanical properties and microcrack/porosity morphology on residual stresses will be examined in future publications by using *OOF* on similar model microstructures. Work is also in progress for measuring the localized residual stresses using stress-induced peak shifts of micro-Raman spectra and fluorescence *R*-lines of $Cr^{3+}$ in alumina. Results are to be correlated with *OOF* simulations.

**Acknowledgments:** The authors thank Dr. J. A. Haynes of ORNL for the micrograph of the TBC system. CHH and PFB acknowledge support of the U.S. Department of Energy, Division of Materials Sciences, Office of Basic Energy Sciences, under contract DE-AC05-96OR22464 with Lockheed Martin Energy Research Corp.; ERF and WCC acknowledge support of the NIST Ceramic Coating Program.

## References

[1] R. A. Miller, "Current Status of Thermal Barrier Coatings-An Overview," *Surf. Coat. Technol.*, **30** [1], 1-11 (1987).

[2] W. Y. Lee, D. P. Stinton, C. C. Berndt, F. Erdogan, Y. D. Lee and Z. Mutasim, "Concept of Functionally Graded Materials for Advanced Thermal Barrier Coating Applications," *J. Am. Ceram. Soc.*, **79** [12], 3003-3012 (1996).

[3] J. A. Haynes, E. D. Rigney, M. K. Ferber, and W. D. Porter, "Oxidation and Degradation of a Plasma-Sprayed Thermal Barrier Coating System," *Surf. Coat. Technol.*, **86-87**, 102-108 (1996).

[4] R. J. Christensen, V. K. Tolpygo and D. R. Clarke, "The Influence of the Reactive Element Yttrium on the Stress in Alumina Scales Formed by Oxidation," *Acta Mater.*, **45** [4], 1761-1766 (1997).

[5] D. J. Wortman, B. A. Nagaraj and E. C. Duderstadt, "Thermal barrier coatings for gas turbine use," *Mater. Sci. Eng.*, **A121**, 433-440 (1989).

[6] J. T. DeMasi-Marcin, K. D. Sheffler and S. Bose, "Mechanisms of degradation and failure in plasma-deposited thermal barrier coating," *J. Eng. Gas Turbines Power*, **112**, 521-526 (1990).

[7] R. A. Miller and C. E. Lowell, "Failure mechanisms of thermal barrier coatings exposed to elevated temperatures," *Thin Solid Films*, **95**, 265-273 (1982).

[8] M. J. Lance, J. A. Haynes, W. R. Cannon and M. K. Ferber, "Piezospectroscopic Characterization of Thermal Barrier Coatings," *Ceramic Transactions*, Volume **89**: Nondestructive Evaluation of Ceramics, edited by C. H. Schilling and J. N. Gray.

[9] A. H. Bartlett and R. Dal Maschio, "Failure mechanisms of a zirconia-8wt% yttria thermal barrier coating," *J. Am. Ceram. Soc.*, **78** [4], 1018-1024 (1995).

[10] C. H. Hsueh and A. G. Evans, "Residual Stresses in Metal/Ceramic Bonded Strips," *J. Am. Ceram. Soc.*, **68** [5], 241-248 (1985).

[11] C. H. Hsueh and A. G. Evans, "Oxidation Induced Stresses and Some Effects on the Behavior of Oxide Films," *J. Appl. Phys.*, **54** [11], 6672-6686 (1983).

[12] J. A. Haynes, M. K. Ferber and E. D. Rigney, "Mechanical properties and fracture behavior of interfacial alumina scales on plasma-sprayed thermal barrier coatings," submitted to *Materials at High Temperatures*, February 1998.

[13] S. A. Langer, W. C. Carter and E. R. Fuller, Jr., "Object Oriented Finite Element Analysis for Materials Science," Center for Theoretical and Computational Materials Science and the Information Technology Laboratory at the National Institute of Standards and Technology, 1997. URL: http://www.ctcms.nist.gov/~wcraig/oof/.

[14] R. V. Hillery, B. H. Pilsner, R. L. McKnight, T. S. Cook, and M. S. Hartle, "Thermal barrier coating life prediction model development," NASA Contractor Report 180807 (1988).

[15] J. A. Haynes, M. K. Ferber, W. D. Porter and E.D. Rigney, "Characterization of alumina scales formed during isothermal and cyclic oxidation of plasma-sprayed TBC systems at 1150°C," submitted to *Oxid. Met.*, February 1998.

[16] G. C. Chang, W. Phucharoen, and R. A. Miller, "Behavior of thermal barrier coatings for advanced gas turbine blades," *Surf. Coat. Technol.*, **30**, 13-28 (1987).

[17] W. Phucharoen, "Development of an analytical-experimental methodology for predicting the life and mechanical behavior of thermal barrier coatings," Ph.D. Thesis, Cleveland State University (1990).

[18] G. J. Petrus and B.L. Ferguson, "A software tool to design thermal barrier coatings: a technical note," *J. Thermal Spray Technol.*, **6**, 29-34 (1997).

**Correspondence.** e-mail: edwin.fuller@nist.gov FAX: (301) 975-5334